

X-ray pulsations from the radio-quiet gamma-ray pulsar in CTA 1¹

P.A. Caraveo, A. De Luca^{1,2}, M. Marelli³, G.F. Bignami¹

INAF - Istituto di Astrofisica Spaziale e Fisica Cosmica, Via Bassini 15, I-20133 Milano,
Italy

pat@iasf-milano.inaf.it

and

P.S. Ray

Space Science Division, Naval Research Laboratory, Washington, DC 20375-5352, USA

and

P. M. Saz Parkinson

Santa Cruz Institute for Particle Physics, University of California Santa Cruz, CA 95064,
USA

and

G. Kanbach

Max-Planck Institut für Extraterrestrische Physik, 85748 Garching, Germany

Received _____; accepted _____

¹Istituto Universitario di Studi Superiori (IUSS) di Pavia, Viale Lungo Ticino 56, I-27100 Pavia (Italy)

²Istituto Nazionale di Fisica Nucleare, Sezione di Pavia, Via Bassi 6, I-27100 Pavia (Italy)

³Università degli Studi dell'Insubria, Via Ravasi 2, 21100 Varese, Italy

ABSTRACT

Prompted by the Fermi LAT discovery of a radio-quiet gamma-ray pulsar inside the CTA 1 supernova remnant, we obtained a 130 ks XMM-Newton observation to assess the timing behavior of this pulsar.

Exploiting both the unprecedented photon harvest and the contemporary Fermi LAT timing measurements, a 4.7σ single peak pulsation is detected, making PSR J0007+7303 the second example, after Geminga, of a radio-quiet gamma-ray pulsar also seen to pulsate in X-rays. Phase-resolved spectroscopy shows that the off-pulse portion of the light curve is dominated by a power-law, non-thermal spectrum, while the X-ray peak emission appears to be mainly of thermal origin, probably from a polar cap heated by magnetospheric return currents, pointing to a hot spot varying throughout the pulsar rotation.

Subject headings: stars: neutron — pulsars: individual (PSR J0007+7303)

1. Introduction

The Fermi LAT discovery (Abdo et al. 2008) of a pulsed gamma-ray signal from the position of the candidate neutron star (NS) RXJ0007.0+7303 (Halpern et al. 2004) inside CTA 1, a 5,000 to 15,000 y old supernova remnant (SNR) at a distance of 1.4 ± 0.3 kpc (Pineault et al. 1993), heralded a new era in pulsar astronomy. Besides fostering an extraordinary increase in the number of pulsars detected in gamma rays, the Fermi LAT first pulsar catalogue (Abdo et al. 2010a) marks the birth of new pulsar sub-families, such as millisecond (Abdo et al. 2009a) and the radio-quiet gamma-ray pulsars (Abdo et al. 2009b). Indeed, with the recent detection of 8 new objects (Saz Parkinson et al. 2010) the gamma-ray discovered pulsars now account for one third of the pulsating NSs seen by Fermi (Caraveo 2010; Ray & Saz-Parkinson 2010). While the detection of so many radio-quiet objects points to a gamma-ray beaming covering a solid angle much larger than the radio one, one wonders if the difference between radio-quiet and radio-loud gamma-ray pulsars is just a geometrical one.

X-ray astronomy offers an independent way to study NSs by assessing their non-thermal magnetospheric emission together with the temperature and emitting area on their surface. Previous X-ray studies of CTA 1 central regions unveiled a central filled SNR (ASCA and ROSAT observations, Seward (1995)) and a point source (Chandra and a short XMM observations, Slane et al. (2004); Halpern et al. (2004)), with a jet-like feature, embedded in a compact nebula. Standard FFT searches on the XMM data failed to detect pulsation, mainly owing to the source faintness. Redoing the exercise using the Fermi LAT timing information yielded unconvincing results, thus prompting the request of a long XMM-Newton observation.

¹Based on observations with XMM-Newton, an ESA science mission with instruments and contributions directly funded by ESA member states and the USA (NASA).

Searching for the source pulsation was, indeed, the main goal of our 130 ks long XMM-Newton observation. The unprecedented harvest of X-ray photons, while unveiling the Fermi LAT periodicity, allowed also for a new detailed study of the source spectral shape.

Using the newly acquired timing and spectral information, we compare the X-gamma behavior of this puzzling radio quiet NS with well known X-ray emitting gamma-ray pulsars.

2. Observations and data reduction

Our deep XMM-Newton observation of the CTA 1 system started on 2009, March 7 at 15:11:10 UT and lasted 130.1 ks. The pn camera (Strueder et al. 2001) of the EPIC instrument was operated in Small Window mode (time resolution of ~ 5.6 ms over a $4' \times 4'$ field of view), while the MOS detectors (Turner et al. 2001) were set in Full frame mode (2.6 s time resolution on a $15'$ radius field of view). We used the XMM-Newton Science Analysis Software v8.0. After standard data processing (using the `epproc` and `emproc` tasks) and screening of high particle background time intervals (following De Luca & Molendi 2004), the good, dead-time corrected exposure time is 66.5 ks for the PN and 93.5 ks for the two MOS. The resulting 0.3-10 keV MOS image is shown in Figure 1. In order to get a sharp view of the diffuse emission in the CTA 1 system, we also used a Chandra/ACIS (Garmire et al. 2003) observation of the field, performed on 2003, April 13 (50.8 ks observing time - such dataset was included in the investigation by Halpern et al. 2004). We retrieved “level 2” data from the Chandra Science Archive and used the Chandra Interactive Analysis of Observation (CIAO) software v3.2.

2.1. Spatial-spectral analysis

The angular resolution of XMM-Newton telescopes' is not sufficient to resolve the pulsar (PSR) from the surrounding pulsar wind nebula (PWN). Thus, we used the spatial-spectral deconvolution method developed by Manzali et al. (2007) to disentangle the point source from the diffuse emission, taking advantage of their different spectra and angular distribution.

1. for each EPIC instrument, we extracted spectra from three concentric regions of increasing radii (0-5", 5"-10", 10"-15").
2. based on the well known angular dependence of the EPIC Point Spread Function (PSF), we estimated the PSR encircled fraction in each region. Since the target is on-axis and most of the counts are below 1 keV, we used PSF model parameters for an energy of 0.7 keV and null off axis angle.
3. We used Chandra data to compute the PWN encircled fraction in each region. To this aim, we simulated the PSR point spread function using the ChaRT² and MARX³ software packages, assuming the PSR spectrum published by Halpern et al.(2004). We positioned the simulated point source at the actual PSR coordinates observed by ACIS, and we normalized it in order to match the observed peak counts in the ACIS image. Then, we subtracted the simulated image from the observed one. This yields an image of the diffuse emission surrounding the pulsar. However, assuming pure pulsar emission at the image peak likely results in underestimating the inner ($r \lesssim 1.5''$) PWN. To correct the residual image for such an effect, we decided to replace

²<http://cxc.harvard.edu/chart/>

³<http://space.mit.edu/CXC/MARX/>

counts in the inner $1.5''$ with a poissonian distribution having a mean value equal to the average number of counts in the $1.5'' - 5''$ surrounding annulus. As a last step, following Manzali et al.(2007), we degraded the angular resolution to match the EPIC PSF, obtaining a map of the PWN surface brightness as seen by EPIC.

4. we fit a two component (PSR+PWN) model to all spectra, freezing the PSR and PWN normalization ratios to the results of the previous steps. Uncertainty in best fit parameters induced by errors in the encircled fractions is estimated to be negligible with respect to statistical errors.

Accounting at once for both the PSR and the PWN, such an approach yields best fit parameters for both spectral models. A more detailed description of the method can be found in Manzali et al. (2007). Together with the XMM spectra, we fitted the spectra obtained from the pulsar ($1.5''$ circle radius) and the nebula ($15''$ circle radius) in the Chandra observation. We used CIAO 4.1.2 software `acispec` to generate the spectrum as well as the response and effective areas.

We focus here into the spectral analysis (step 4). Background spectra for each EPIC camera were extracted from source-free regions within the same chip. Ad-hoc response and effective area files were generated using the SAS tasks `rmfgen` and `arfgn`. Since in our approach encircled energy fractions for the PSR and PWN are computed a priori and then used in the spectral analysis, effective area files are generated with the prescription for extended sources, without modelling the PSF distribution of the source counts. Spectra from the three regions were included in a simultaneous fit using the combination:

$$(\text{interstellar absorption}) \times (\rho_i(\text{PSR model}) + \epsilon_i(\text{PWN model}))$$

where ρ_i and ϵ_i are the PSR and PWN encircled fractions within the i^{th} extraction region.

The interstellar absorption coefficient does not depend on i . For the PWN, we used a power law model. Although the PWN spectrum is expected to vary as a function of the position, the relatively small photon statistic prompted us to fit a single photon index Γ_{PWN} to all regions. Of course, PSR parameters do not vary in the different annuli. For the PSR emission, we tried a simple power law, the combination of a power law and a blackbody as well as the combination of a power law and a magnetized neutron star atmosphere model (*nsa* in XSpec - assuming a $1.4 M_{\odot}$ neutron star with a radius of 13 km and a surface magnetic field of 10^{13} G).

All the models for the PSR emission yield statistically acceptable fits (power law: $\chi^2_{\nu}=91.5$, 124 d.o.f.; blackbody+power law: $\chi^2_{\nu}=85.8$, 121 d.o.f.; *nsa*+power law: $\chi^2_{\nu}=86.8$, 121 d.o.f.).

The resulting parameters are summarized in Table 1. As expected, the *nsa* model yields smaller temperatures and larger emitting areas than the blackbody model.

Using the best fit blackbody+power law model, within a $15''$ circle in 0.3-10 keV, we estimate that 47% of the pn counts come from the PSR, 32% from the PWN and 21% are background (instrumental as well as cosmic).

In order to discriminate between the purely non-thermal and the composite (thermal + non-thermal) description of the pulsar emission, the high resolution, temporal information provided by the pn instrument is crucial.

2.2. Timing Analysis

4989 pn events in the 0.15-10 keV energy range were extracted from a $15''$ circle, centered on the gamma-ray pulsar. PATTERN selection was performed as by Pellizzoni et al. (2008). X-ray photons' times of arrival were barycentered according to the PSR Chandra position (RA 00:07:01.56, Dec 73:03:08.3) and then folded according to an accurate Fermi-LAT timing solution (Abdo et al. 2010a) that overlap our XMM dataset (the pulsar period at the start of our XMM-Newton observation is $P=0.3158714977(3)$ s). Such exercise was repeated selecting photons in different energy ranges.

A 4.7σ pulsation is seen in the 0.15-2 keV energy range (null hypothesis probability of 1.1×10^{-6} , according to a χ^2 test), characterized by a single peak, which is out of phase with respect to the gamma-ray emission. Light curves computed for different energy ranges are shown in Figure 2, phase aligned with the gamma-ray one.

Results from the previous section make it possible to compute a net (background and PWN - subtracted) pulsed fraction of $85 \pm 15\%$ in the 0.15-0.75 keV energy range. No pulsation is seen in the 2-10 keV energy range. Assuming a sinusoidal pulse profile, we evaluated a 3σ upper limit of 57% on the net pulsed fraction. Such a difference in the overall source pulsation as a function of the photon energy does not support the single-component model for the PSR emission, pointing to the composite thermal plus power law model.

2.3. Phase-resolved spectroscopy

Phase-resolved spectral analysis was performed by selecting on- and off-pulse portions of the light curve. We selected pn events ($15''$ extraction radius, PATTERN 0) from the phase intervals corresponding to the peak and to the minimum of the folded light curve. These spectra are plotted in Figure 4 where they are seen to differ only at low energy,

while they appear superimposed for $E > 1.2$ keV. We adopted the best fit model computed in sect. 2.1, featuring the composite black-body + power-law spectrum for the PSR, as a template to describe the phase-resolved spectra. Following Caraveo et al. (2004) and De Luca et al. (2005), we fixed all spectral parameters (including the PWN component) at their phase-averaged best fit values and we used the the normalizations of the PSR thermal and non-thermal components to describe the pulse-phase modulation. The spectral variation may be well described as a simple modulation of the emitting radius of the thermal component, keeping the power law component fixed ($\chi^2 = 26.2$, 31 d.o.f. for the blackbody+power law model; $\chi^2 = 25.9$, 31 d.o.f. for the *nsa*+power law model). Using the blackbody model, the emitting radius of the thermal component varies from 242_{-242}^{+111} m to 600_{-75}^{+68} m as a function of the star rotation phase. Using the *nsa* description, the emitting radius varies from 560_{-560}^{+720} m to 4380_{-1150}^{+740} m. Quoted values of the emitting radii are as measured from a distant observer. Such a variation could easily account for the totality of the X-ray pulsation.

Fitting the on-off spectra using a single power law component does not yield acceptable results ($\chi^2 = 48.9$, 31 d.o.f.), while the paucity of the counts does not allow to test a model where both thermal and non-thermal components are allowed to vary.

2.4. Extended emission spectral analysis

Diffuse emission, already discovered by ROSAT and ASCA (Halpern et al. 2004; Slane et al. 2004), pervades the entire EPIC/MOS field of view. A thorough analysis of such emission, requiring ad-hoc background subtraction/modelling techniques, is beyond the scope of this paper, focused the pulsar phenomenology. For completeness, we include a simple study of the inner and brighter portion of the diffuse emission (within $\sim 150''$ from the pulsar). Using the brightness profile along different radial directions, we selected

two elliptical regions (ellipse 1 and 2, see Figure 1) – excluding the inner 15'' radius circle – and we extracted the corresponding spectra from the MOS data. Background spectra were extracted from a region outside ellipse 2. Since ellipse 1 lies within the pn field of view, we extracted also a pn spectrum for such a region. Owing to the dimension of the pn field of view, the pn background spectrum was extracted from a region within ellipse 2. However, the difference in surface brightness between the two ellipses is large enough to induce a negligible distortion to the pn ellipse 1 spectrum. The extended emission is well described by a power law spectrum with an index of 1.59 ± 0.18 in the inner portion (ellipse 1, $\chi^2=123.9$, 90 dof) and of 1.80 ± 0.09 in the outer portion (ellipse 2, $\chi^2=189.3$, 137 dof). The observed flux is of $1.60 \pm 0.09 \times 10^{-13}$ erg cm $^{-2}$ s $^{-1}$ and of $1.98 \pm 0.06 \times 10^{-12}$ erg cm $^{-2}$ s $^{-1}$ for the inner and outer portions, respectively. Owing to smaller collecting area as well as larger background per unit solid angle, Chandra/ACIS data yield consistent, although less constrained, results for such an extended emission.

3. Discussion and Conclusions

After Geminga, PSR J0007+7303 now becomes the second example of a radio-quiet gamma-ray pulsar also seen to pulsate in X-rays.

Our deep XMM-Newton observation characterizes the system emission as follows.

The PWN X-ray spectrum at the position of the pulsar can be described by a power law with index $\Gamma_{PWN} = 1.5 \pm 0.3$. Diffuse, non-thermal emission with a decreasing surface brightness is seen across the EPIC field of view, with a photon index steepening as a function of the distance from the pulsar ($\Gamma = 1.80 \pm 0.09$ at 1 ÷ 2.5 arcmin distance).

The X-ray spectrum of the pulsar is a combination of thermal radiation superimposed to a non-thermal power law component. Thermal emission comes from a “hot spot”, larger

than the polar cap computed for a dipole model for PSR J0007+7303 (about 100 m radius), but significantly smaller than the entire surface of any reasonable NS. This is true both using the blackbody model and the neutron star atmosphere model (see Table 3), although the latter yields a larger emitting area and a lower temperature. Indeed, we warn that for some thermally emitting PSR the use of the *nsa* model turned out to be problematic (see e.g. the case of PSR B0656+14 discussed by De Luca et al. 2005). Thus, *nsa* results should be taken with caution. At variance with the majority of X-ray emitting isolated pulsars (e.g. Kaspi et al. (2006)), no thermal component from the whole NS surface is discernible from the XMM spectrum. Using the blackbody model, the 3σ upper limit on the temperature of a 10 km radius NS is 5.3×10^5 K and 4.8×10^5 K using the *NSA* model. This makes PSR J0007+7303 by far the coldest NS for its age interval, suggesting a rapid cooling for this young gamma-ray pulsar.

The detection of X-ray pulsation makes it possible to directly compare the PSR J0007+7303 multiwavelength phenomenology with that of other prototypical pulsars.

With a rotation energy loss of $4.52 \times 10^{35} \text{ ergs}^{-1}$ and a kinematic age of 13 ky, PSRJ0007+7303 is 50 times younger and 10 times more energetic than Geminga, for many years the only known radio-quiet gamma-ray pulsar (for a review, see Bignami & Caraveo, 1996). While PSR J0007+7303 is a relatively young, Vela-like pulsar, its rotational energy loss is intermediate between Geminga and Vela. Thus, it makes sense to compare PSR J0007+7303 with Vela and Geminga, two NSs with a well established multiwavelength phenomenology (Sanwal et al. 2002; Manzali et al. 2007; Caraveo et al. 2004; De Luca et al. 2005; Jackson et al. 2005).

Starting from the source flux values, if we consider the ratio between the gamma-ray and non-thermal X-ray fluxes, we find a value of $(5.6 \pm 1.1) \times 10^3$ for CTA 1, to be compared with $(6.8 \pm 0.4) \times 10^3$ for Geminga and $(1.3 \pm 0.3) \times 10^3$ for Vela. Thus, the young and

energetic gamma-ray pulsar PSR J0007+7303 is somewhat under-luminous in X-rays, joining Geminga and PSR J1836+5925, another radio-quiet pulsar also known as Next Geminga (Halpern et al. 2007; Abdo et al. 2010b).

Turning now to the phase resolved spectral analysis, we note that the peak emission of the newly measured single-peak X-ray light curve can be ascribed to a hot spot, apparently varying throughout the pulsar rotation. Although the hot spot dimension seems too big to be reconciled with the NS polar cap, but too small to account for the entire NS surface, the varying thermal contribution is indeed reminiscent of the behavior of middle-aged pulsars such as Geminga and PSR B1055-52 (De Luca et al. 2005) .

Although PSR 0007 is the second radio quiet NS seen to pulsate in X-ray, we note that the X-to-gamma-ray observational sequence, which was successfully applied with Geminga, has been reversed. Here, for the first time, the basic pulsar properties (P , \dot{P}) were discovered through the gamma-ray emission which made it possible the detection of the source X-ray pulsations.

While X-ray observations of gamma-ray pulsars remain crucial to probe the source physics, the superb sensitivity of the Fermi LAT has made the discovery of periodicities far more fruitful in the gamma-ray band, as shown by Abdo et al. (2009b) and Saz Parkinson et al. (2010).

This work was supported by contracts ASI-INAF I/088/06/0 and NASA NIPR NNG10PL01I30.

Facilities: XMM (EPIC), CXO (ACIS).

REFERENCES

- Abdo, A., A., et al., 2008, *Science* 322, 1218
- Abdo, A., A., et al., 2009a, *Science* 325, 848
- Abdo, A., A., et al., 2009b, *Science* 325, 840
- Abdo, A., A., et al., 2010a, *ApJS* 187, 460
- Abdo, A., A., et al., 2010b, *ApJ* 712, 1209
- Bignami, G.F. & Caraveo, P.A., *ARA&A* 34, 331
- Caraveo, P.A., 2010, in *High Time Resolution Astrophysics (HTRA) IV*, Agios Nikolaos, Crete (Greece), May 5 - 7, 2010, arXiv:1009.2421
- Caraveo, P.A., et al., 2004, *Science* 305, 376
- De Luca, A., et al., 2005, *ApJ* 623, 1051
- De Luca, A. & Molendi, S., 2004, *A&A* 419, 837
- Garmire, G., et al., 2003, *SPIE* 4851, 28
- Halpern, J.P., et al., 2004, *ApJ* 612, 398
- Halpern, J.P., et al., 2007, *ApJ* 668, 1154
- Jackson, M.S., et al., 2005, *ApJ* 633, 1114
- Kaspi, V., et al., 2006, in “Compact Stellar X-ray Sources”, eds. Lewin, W. and van der Klis, M., Cambridge University Press, p. 279
- Manzali, A., et al., 2007, *ApJ* 669, 470

Pellizzoni, A., et al., 2008, ApJ 679, 664

Pineault, S., et al., 1993, AJ 105, 1060

Ray, P.S. & Saz-Parkinson, P., 2010, Proceedings of ICREA Workshop “The High-Energy Emission from Pulsars and their Systems”, arXiv:1007.2183

Sanwal, D. et al. 2002, ASPC, 271, 353

Saz Parkinson, P., et al., 2010, submitted to ApJ, arXiv:1006.2134

Seward, F. et al. 1995, A&A, 453, 284

Slane, P., et al., 2004, ApJ 601, 1045

Strueder, L., et al., 2001, A&A 365, L18

Turner, M., et al., 2001, A&A 365, L27

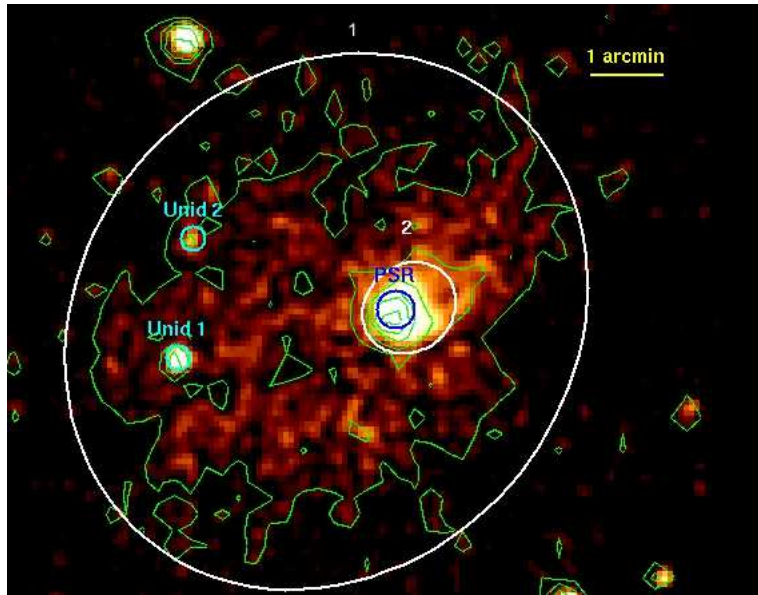


Fig. 1.— 0.35-10 keV MOS Imaging. The two MOS exposure-corrected images have been added and smoothed with a Gaussian with a Kernel Radius of $13''$. The two white ellipses indicate the extended source and the compact PWN. A $15''$ blue circle indicates the PSR position while two unidentified sources are marked with cyan circles.

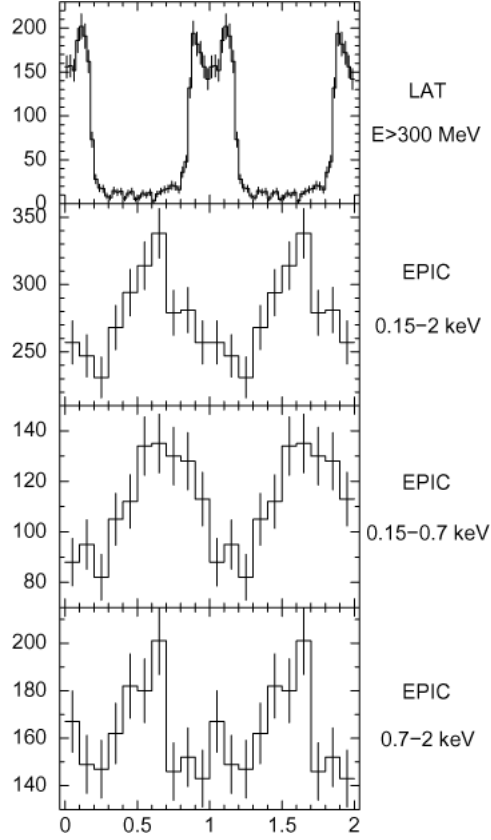


Fig. 2.— EPIC/pn folded light curves in different energy ranges using photons within a $15''$ radius from the Chandra position. X-ray photons’ phases were computed according to an accurate Fermi-LAT ephemeris overlapping with the XMM dataset: the pulsar period at the start of the XMM observation is $P=0.3158714977(3)$ s and the \dot{P} contribution was taken in account. PATTERN 0 events have been selected in the 0.15-0.35 keV energy range while PATTERN ≤ 4 have been used in the 0.35-2 keV range. The upper panel shows the LAT light curve of the CTA 1 pulsar from Abdo et al. (2010a) to which the XMM light curves have been aligned in phase.

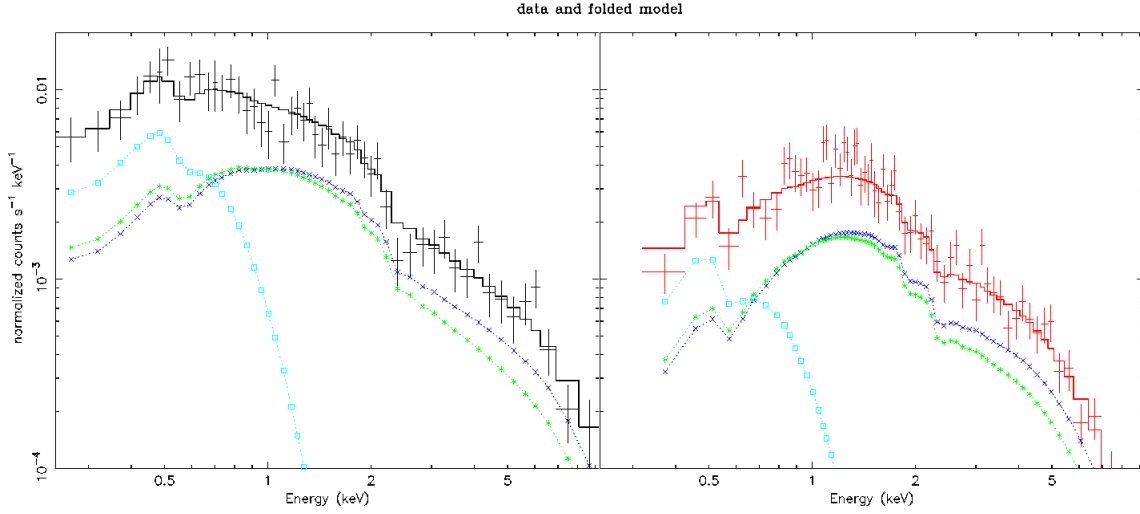


Fig. 3.— PN and MOS spectra of PSR J0007+7303. PATTERN 0 PN events and PATTERN ≤ 12 MOS events have been selected among photons within $15''$ from the target position. The spectra are rebinned in order to have at least 25 counts per bin and no more than 3 spectral bins per energy resolution interval. The black and the red curves show respectively the PN and MOS data and spectral fits. Cyan square-marked curve shows the blackbody component, while pulsar power law is shown with blue curves and PWN one with green asterisks.

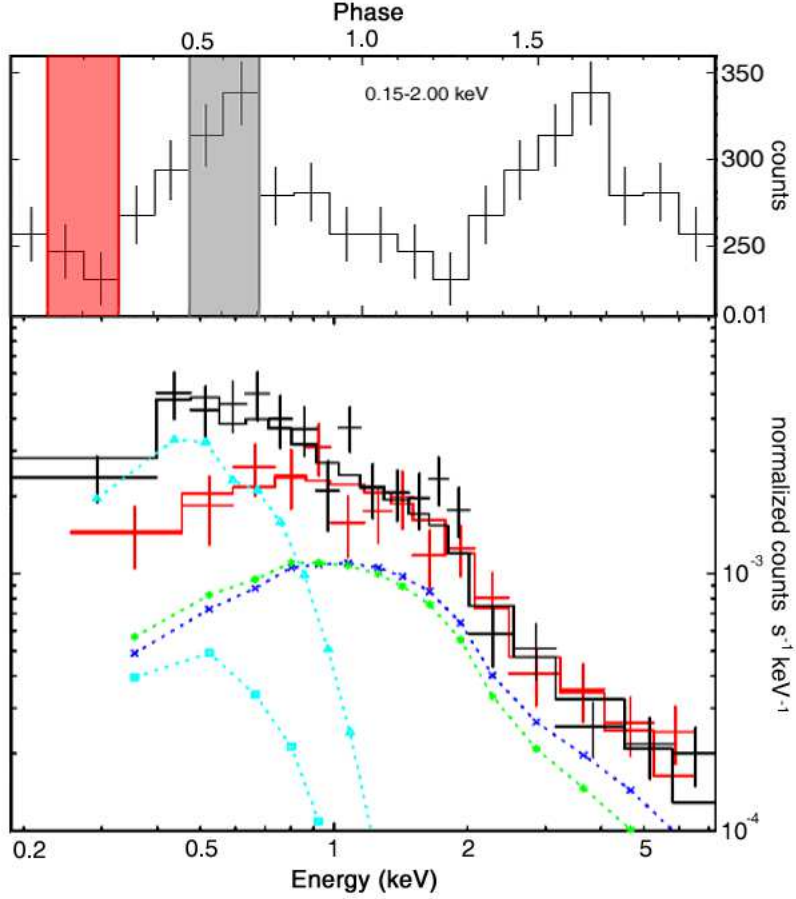


Fig. 4.— Upper panel: X-ray folded light curve of PSR J0007+7303 (0.15-2 keV). Lower panel: X-ray spectra relative to the phase intervals shaded in gray (on-pulse, black line) and red (off-pulse, red line). Both spectra were fitted with a 3-component model to account for the NS thermal emission (cyan symbols) and power law (blue dotted line) as well as the PWN power law (green dotted line). With the power law contributions unchanged in the two spectra, a significant thermal component is present only in the on-pulse spectrum (cyan triangles) while it appears suppressed in the off-pulse one (cyan squares).

Table 1: CTA 1 Pulsar and nebula spectra.

Parameter	Pulsar J0007+7303			Inner PWN	Outer PWN
	PL	PL+BB	PL+NSA		
$N_H(10^{21})$	$0.63^{+0.25}_{-0.23}$	$1.66^{+0.89}_{-0.76}$	$1.53^{+1.19}_{-0.73}$	$1.67^{+1.38}_{-1.22}$	$1.83^{+0.30}_{-0.27}$
Γ_{PWN}	$1.25^{+0.17}_{-0.15}$	$1.53^{+0.33}_{-0.27}$	$1.49^{+0.32}_{-0.24}$	1.59 ± 0.18	1.80 ± 0.09
Γ_{PSR}	$1.36^{+0.16}_{-0.14}$	1.30 ± 0.18	$1.25^{+0.20}_{-0.19}$	-	-
kT(keV)	-	$0.102^{+0.032}_{-0.018}$	$0.054^{+0.025}_{-0.016}$	-	-
$r_{1.4kpc}(\text{km})$	-	$0.64^{+0.88}_{-0.20}$	$4.92^{+1.81}_{-4.68}$	-	-
χ^2	91.56	85.81	86.82	123.89	189.30
d.o.f.	124	121	121	90	137
Total Flux $_{0.3-10keV}^a$	12.00 ± 0.10	13.90 ± 0.36	14.01 ± 0.41	16.0 ± 0.9	198 ± 6
Total Flux $_{2-10keV}^a$	$8.83^{+0.37}_{-0.28}$	$8.69^{+0.97}_{-0.86}$	$8.74^{+1.02}_{-0.91}$	10.1 ± 0.6	105 ± 5
PSR Flux $_{0.3-10keV}^a$	6.54 ± 0.53	8.41 ± 0.98	8.41 ± 1.00	-	-
PSR Flux $_{2-10keV}^a$	3.98 ± 0.72	$4.30^{+1.62}_{-0.61}$	$4.32^{+1.67}_{-0.65}$	-	-
Thermal Flux a	-	1.55 ± 1.01	1.68 ± 1.11	-	-

Note. — X-ray spectrum of the pulsar and the nebula. Inner and Outer PWN correspond to emission from ellipse 1 and ellipse 2, respectively (see text and Figure 1). For the pulsar we provide the power law, the blackbody + power law and the magnetized neutron star atmosphere model (*nsa*) + power law spectral fits. Temperatures and emitting radii are as measured from a distant observer. For the pulsar and inner nebula we used Chandra, MOS and PN data, while for the outer PWN spectra we used only data from MOS1+2 instruments owing to the small FOV of PN.

^a Fluxes are in units of $10^{-14} \text{erg/cm}^2 \text{s}$